

Millimeterwave (60 GHz) Imaging Wireless Sensor Network: Recent Progress

Munkyo Seo, Bharath Ananthasubramaniam, Upamanyu Madhow and Mark J. W. Rodwell
Department of Electrical and Computer Engineering
University of California,
Santa Barbara, CA 93106-9560, Email: mkseo@engineering.ucsb.edu

Abstract—In this paper, we report recent progress on an experimental 60-GHz wireless sensor network based on an virtual imaging approach. The results of indoor radio experiments, including the bit-error-rate (BER) and sensor range measurements, are discussed. Basic link tests of low-power CMOS sensors are also presented.

I. INTRODUCTION

Sensor networks provide distributed information collection and transmission, and are useful for many industrial, environmental or military applications. Conventional wireless sensor networks (WSN) typically rely on multi-hop communication among neighboring sensors for information gathering (Fig. 1). For the purpose of sensor localization, various techniques exist, including measuring time-of-flight (of either radio or acoustic waves), using GPS, etc. It is known that the conventional approach based on multi-hop data transfer can be inefficient when the network size or the number of sensors are very large. It also tends to make sensor hardware rather complicated, especially if ranging devices are to be integrated.

As an alternative to the conventional WSN, a simplistic approach to wireless sensor networks has been proposed [1]–[3]. In this architecture, sensors retain minimal functionality with no localization or network capability. This will enable ultimate cost and energy efficiency in favor of a very large scale network. The system complexity (or functionality) is instead moved to an information collector, whose spatially narrow radio beam selectively activates a subset of sensor nodes. Fig. 2 illustrates the proposed network architecture. First, the collector beam sequentially scans a sensor field. Second, illuminated sensors respond to the beacon by appropriately modulating and sending it back to the collector. Finally, the collector, upon completing a full scan, acquires an information map across the sensor field. The location of each sensor can also be accurately determined by using a wide bandwidth, spatially narrow beacon in analogy to radar. The return signal, however, also carries local data from possibly a number of sensors, unlike conventional radar. Furthermore, sensors intentionally shift the frequency of the received beam to differentiate their transmission signal with direct ground return or environmental reflections. The proposed sensor net can also be interpreted as a virtual imaging network: image map is drawn from reflected light by a large number of target pixels.

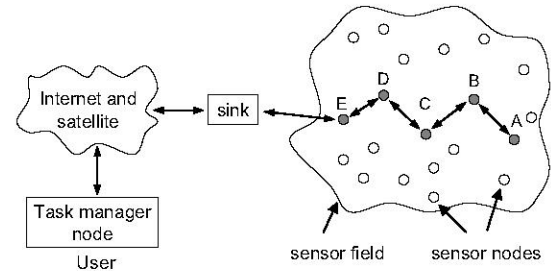


Fig. 1. A Multi-hop based wireless sensor network. After [4].

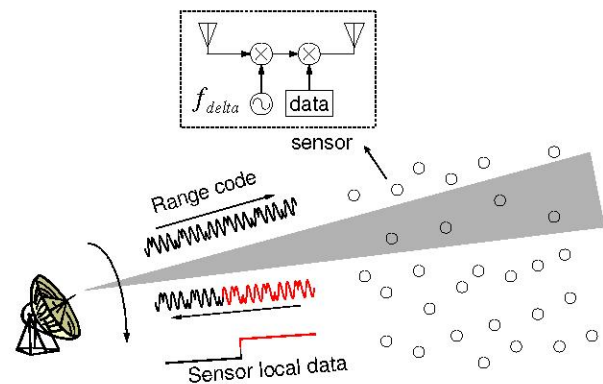


Fig. 2. Imaging sensor network architecture

In this paper, we present recent progress on the millimeter-wave imaging wireless sensor network, including results from the indoor radio experiments and initial CMOS sensor link test. In the next section, the implementation of the 60 GHz prototype system is briefly reviewed. The results from indoor radio experiments are discussed next. Initial test results of CMOS sensors follow.

II. 60 GHz PROTOTYPE SYSTEM

A. Collector and Sensor Hardware

Fig. 3 shows the block diagram of the prototype collector. The collector is basically a 60-GHz transceiver with steerable high-gain antennas (23 dB and 40 dB for the transmit and receive antenna, respectively). It continuously transmits a wideband range code, i.e. 20 MHz pseudo-random bit

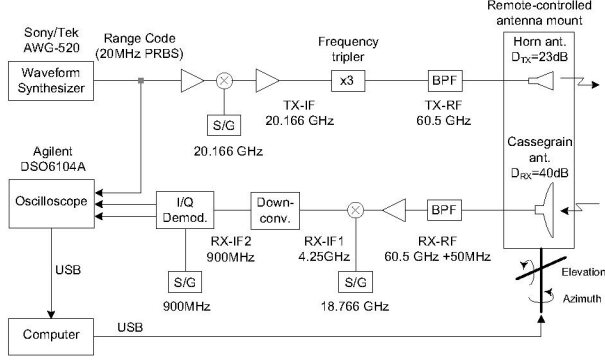


Fig. 3. Block diagram of the 60-GHz prototype collector

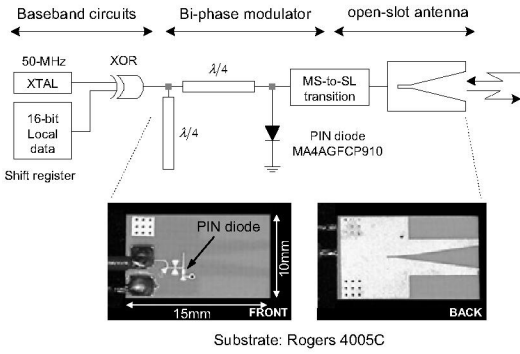


Fig. 4. Block diagram of the 60-GHz prototype sensor

sequence (PRBS) of length $2^6 - 1$ chips. A round-trip distance of a single chip is thus 7.5 m. The range code repeats itself every $3.25 \mu s$, and this guarantees unique determination of the range up to 472.5 m. Reflected signals from sensors are down-converted to the baseband and captured by a four-channel oscilloscope. By taking cross-correlation between the transmit and receive copy of the range-code, the relative distance between the collector and sensors can be measured. Overall, the collector, upon completing a full scan, performs a multi-dimensional matched filtering to the received data to estimate the radial and angular location of the sensor.

Fig. 4 illustrates the equivalent circuit of the 60 GHz prototype passive sensor. The collector beam is received by a linearly-tapered slot-antenna (LTSA) terminated by a PIN diode. The input bias turns on and off the PIN diode, presenting two impedance states with approximately 180 degree phase difference. The beacon is hence reflected with either 0 or 180 degree relative phase shift, and eventually re-transmitted toward the collector. 16-bit local data and 50 MHz shifting LO (to avoid direct ground returns) are simultaneously imposed on diode bias through a XOR gate. The electrical characteristics of open-slot antennas are relatively insensitive to manufacturing tolerances, and are thus suitable for low-cost manufacturing.

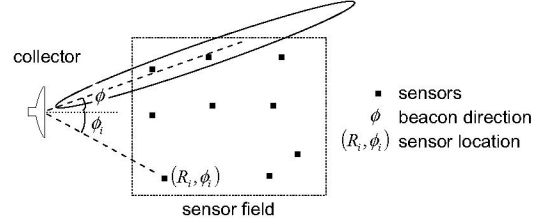


Fig. 5. Imaging sensor net geometry in angular coordinate.

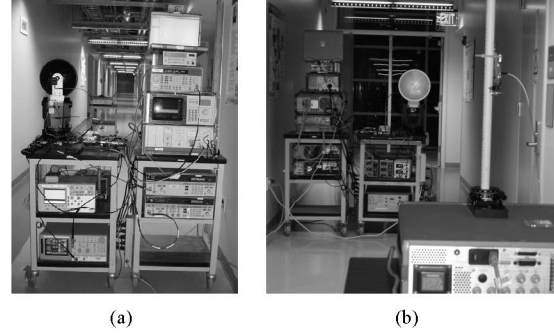


Fig. 6. Indoor radio experiments: the collector system (left) and the view from a sensor (right).

B. Collector Signal Processing

Fig. 5 illustrates the sensor network coordinate with a beam-steerable collector. Only one angular coordinate is considered for simplicity. The discussion however extends to a more general case with two orthogonal angular coordinates for full 3-D localization.

Let $s(t)$ the range code, and $r(t, \phi)$ the collector receive signal as a function of azimuth angle ϕ and time t . Assume the collector is at origin, and a single sensor is located at (R_1, ϕ_1) . $r(t, \phi)$ is then represented as

$$r(t, \phi) = G(\phi - \phi_1) s(t - R_1/2c) + n(t), \quad (1)$$

where $G(\phi)$ and $n(t)$ is the antenna gain function (AGF) and Gaussian noise, respectively. The maximum-likelihood (ML) estimate of the sensor location, $(\tilde{R}_1, \tilde{\phi}_1)$, can be obtained from the observation $r(t, \phi)$ by

$$(\tilde{R}_1, \tilde{\phi}_1) = \arg \min_{(\tilde{R}, \tilde{\phi})} \left\langle G(\phi - \tilde{\phi}), \left| \left\langle r(t, \phi), s\left(t - \tilde{R}/2c\right) \right\rangle_t \right| \right\rangle_{\phi}, \quad (2)$$

where $\langle \cdot \rangle_t$ and $\langle \cdot \rangle_{\phi}$ is taking cross-correlation in t and ϕ , respectively. Equation (2) is essentially 2-D matched filtering, but only the magnitude is taken from the range correlation output. This is because the phase of $r(t, \phi)$ is unknown to the collector. The AGF $G(\phi)$ is equal to the cascade of collector TX and RX antenna radiation pattern. For the present prototype, $G(\phi)$ is almost equal to the RX antenna (40 dB cassegrain) pattern since the TX antenna (23 dB horn) has a much wider 3 dB beamwidth.

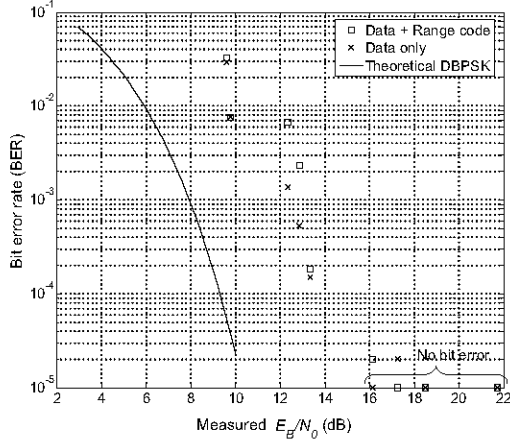


Fig. 7. Measured BER performance at the sensor data rate of 100 Kbps (based on observing 100,000 bits)

III. INDOOR RADIO EXPERIMENTS

Indoor radio experiments (< 9 m) are conducted to evaluate the basic system performance of the proposed millimeterwave imaging sensor network. Photographs of the system under radio experiments are shown in Fig. 6.

A. Bit-Error-Rate Measurement

The collector beam was aimed at the sensor (Fig. 6), and the range between the collector and sensor was varied between approximately 3 m and 9 m. For each range, 100,000 bits of sensor data at 100 Kbps were collected, and the BER is measured. The results are shown in Fig. 7. It is seen that the measured BER follows prediction with 4 dB of E_b/N_0 loss. The most responsible factor for this loss was found to be the increase in the receiver noise floor due to strong echo from indoor environments. The effects of these environmental reflections can be minimized by either increasing the sensor frequency separation (currently 50 MHz) or by operating the system in an outdoor environment. It is also seen in Fig. 7 that the presence of the range code does not significantly affect the BER performance.

In Fig. 7, the estimation of E_b/N_0 was obtained by pure sinusoidal signaling, i.e. by turning off the range-code as well as sensor local data.

B. Range Measurement

The distance between the collector and sensor is measured and plotted against actual sensor locations in Fig. 8. For each sensor location, 20 measurements were performed, where each range measurement is based on observing 500 repetitions of the range code. A range offset of approximately 12.6 m is seen in Fig. 8, which is due to electrical delays (or *group* delays) in the collector transceiver. After subtracting this offset from the measurement, the RMS error in range measurement is obtained as shown in Fig. 9. Under the present experimental conditions, very low-frequency fluctuations in collector group delays are most responsible for the RMS range error. Other sources of

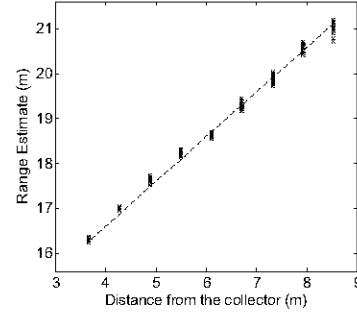


Fig. 8. Measured distance between the collector and sensor. For each sensor location, 20 measurements were carried out.

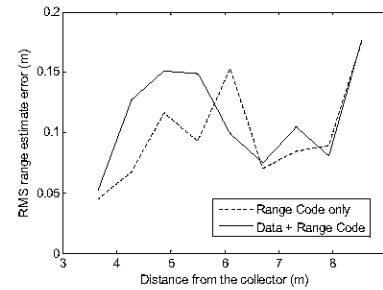


Fig. 9. RMS range measurement error from multiple measurements in Fig. 8.

error include internal range interpolation in collector signal processing, and, more fundamentally, additive white gaussian noise at the receiver.

C. 3-D Localization

Previous BER and range measurement were based on a fixed collector beam angle. After a full 2-D angle scan (in azimuth and elevation), the 3-D location of sensors can be identified. Fig. 10 illustrates such 3-D localization when only one sensor is present. When multiple sensors are present in the field, data demodulation should be performed for each identified sensor location.

IV. LOW-POWER CMOS REFLECTION SENSOR

In a typical wireless sensor network, sensors are subject to severe energy constraints for the requirement of low maintenance, long battery life, etc. The power consumption of the prototype sensor in Fig. 4 is approximately 20 mW, dominated by the PIN diode bias currents. To significantly reduce the dc power consumption, the prototype sensor in Fig. 4 is designed and fabricated in 90-nm CMOS technology. Main building blocks are a low-power ring oscillator and impedance modulator. Flip-chip packaging will provide interface to an external antenna from CMOS sensor. The fabricated CMOS sensors are now under active characterization, but initial measurements showed that ultra low-power operation ($< 10\mu W$) is possible.

Initial link test results of the CMOS sensor is shown in Fig. 11. The sensor chip on a probe station is connected

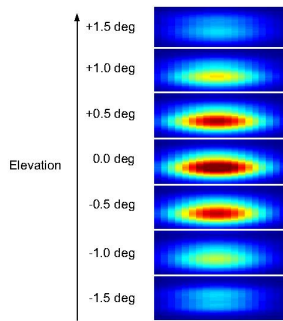
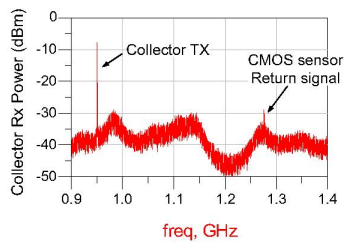


Fig. 10. An example of 3-D sensor localization. Each rectangular image is constructed from the output of 2-D matched filter (in radial and azimuth), and represents a field size of approximately 12 m by 0.6 m. The peak on the map indicates the most probable sensor location.



(a)



(b)

Fig. 11. CMOS sensor link test (left) and the collector IF received spectrum (right). The CMOS sensor is located at 3.5 m away from the collector.

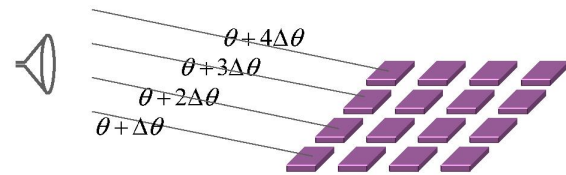
to an external horn antenna (with waveguide interface) for communication with the collector at 3.5 m away from the sensor. Fig. 11(b) shows the received spectrum at the collector IF, where the sensor reflection is 300 MHz away from the collector beam.

V. DISTRIBUTED BEAM-FORMING

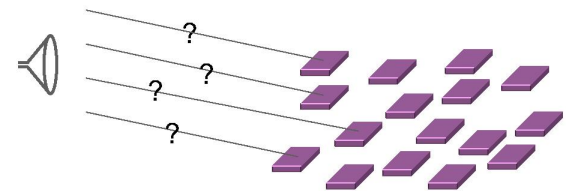
Energy constraints on the sensor node can also severely limit the maximum range that sensors can communicate over. An interesting possibility to extend the communication range, under energy-limited sensor scenarios, is to group a number of neighboring sensors and adding up their transmit power [5]. In other words, a group of near-by sensors can form a *virtual antenna array*, or *distributed phased array* (as opposed to *regular* phased array in Fig. 12). If N sensors collaborate in this way, their aggregate transmit power will increase by a factor of N^2 , extending the communication range by N . The challenge is to make sure individual sensor RF carrier reach the receiver with the same frequency and phase. Recently, a feedback-based approach has been proposed to calibrate static phase misalignments among sensors [6], [7]. An interesting extension of the method to further synchronize sensor local frequencies is also proposed, and will be presented [8].

VI. CONCLUSION AND FUTURE WORK

We have presented recent progress on the millimeterwave (60 GHz) wireless sensor network based on the virtual-



(a) Regular phased array



(b) Distributed phased array

Fig. 12. Regular and *distributed* phased array

imaging approach, including results from the indoor radio experiments and initial CMOS sensor link test.

Currently, the prototype sensor passively reflects the collector beam, without any RF amplification. While this enables simple hardware and low-power operation, the communication of this RFID-like operation is limited to only short distances. Nanoscale CMOS technologies (e.g. 90-nm or below) can provide inexpensive millimeterwave signal amplification, and this will help scale up the size of the network. Design of *active* sensors with RF gain is under investigation.

ACKNOWLEDGEMENTS

This work was supported by the National Science Foundation under grant CCF-0431205 and CNS-0520335, and by the Office of Naval Research under grant N00014-06-1-0066.

REFERENCES

- [1] B. Ananthasubramaniam and U. Madhow, "Virtual radar imaging for sensor networks," *Information Processing in Sensor Networks, 2004. IPSN 2004. Third International Symposium on*, pp. 294–300, 26-27 Apr. 2004.
- [2] —, "On Localization Performance in Imaging Sensor Nets," *Signal Processing, IEEE Transactions on [see also Acoustics, Speech, and Signal Processing, IEEE Transactions on]*, vol. 55, no. 10, pp. 5044–5057, Oct. 2007.
- [3] M. Seo, B. Ananthasubramaniam, M. Rodwell, and U. Madhow, "Millimeterwave Imaging Sensor Nets: A scalable 60-GHz wireless sensor network," *2007 IEEE MTT-S Int. Microwave Symp. Dig.*, pp. 563–566, 3-8 June 2007.
- [4] I. Akyildiz, W. Su, Y. Sankarasubramaniam, and E. Cayirci, "A survey on sensor networks," *Communications Magazine, IEEE*, vol. 40, no. 8, pp. 102–114, Aug. 2002.
- [5] H. Ochiai, P. Mitran, H. Poor, and V. Tarokh, "Collaborative beamforming for distributed wireless ad hoc sensor networks," *IEEE Transactions on Signal Processing*, vol. 53, no. 11, pp. 4110–4124, Nov. 2005.
- [6] R. Mudumbai, J. Hespanha, U. Madhow, and G. Barriac, "Scalable feedback control for distributed beamforming in sensor networks," *Information Theory, 2005. ISIT 2005. Proceedings. International Symposium on*, pp. 137–141, 4-9 Sept. 2005.
- [7] R. Mudumbai, B. Wild, U. Madhow, and K. Ramchandran, "Distributed Beamforming using 1 Bit Feedback: from Concept to Realization," *Proc. of 44th Allerton Conference on Communication Control and Computing*, Sept. 2006.

- [8] M. Seo, M. Rodwell, and U. Madhow, "A feedback-based distributed phased array technique and its application to 60-GHz wireless sensor network," *submitted to 2008 IEEE/MTT-S International Microwave Symposium*.